Fibers and Polymers 2012, Vol.13, No.7, 864-873 DOI 10.1007/s12221-012-0864-7

Investigation of the Effect of Cupric Chloride on Thermal Stabilization of Polyamide 6 as Carbon Fiber Precursor

Ismail Karacan* and Gülçin Baysal

Department of Textile Engineering, Erciyes University, Kayseri, Turkey
(Received December 12, 2011; Revised February 13, 2012; Accepted February 19, 2012)

Abstract: An investigation on the role of cupric (Cu^{2+}) ion incorporation during the thermal stabilization of polyamide 6 fibers was carried out using a combination of differential scanning calorimetry (DSC), thermogravimetric analysis (TGA) and X-ray diffraction (XRD) measurements. Cupric chloride pretreated and thermally stabilized polyamide 6 (PA6) fibers was characterized by a reduction in fiber diameter and linear density values together with color changes from light brown to black with increasing stabilization time. PA6 fibers were properly stabilized after 8 h of stabilization time prior to carbonization. The results obtained from DSC and TGA measurements indicated that there was an improvement in the thermal stability when cupric (Cu^{2+}) ions were incorporated into the polymer structure. TGA thermograms showed the relative improvement in thermal stability as indicated by increasing char yield with progressing time. Char yield reached a maximum value of 33.6 % at 1000 ^{o}C for the cupric chloride pretreated PA6 fibers stabilized for 12 h at 180 ^{o}C. Experimental results obtained from DSC and X-ray diffraction methods suggested the loss of crystallinity as a result of perturbation of hydrogen bonds with progressing time. The formation of cupric ion-amide coordination bonds improved the thermal stabilization by encouraging the development of ladder-like structures. The investigation resulted in a new method of evaluation of X-ray stabilization index specifically intended for the thermally stabilized PA6 fiber.

Keywords: Thermal stabilizaton, Polyamide 6, Carbon fiber, Thermal analysis, X-ray diffraction

Introduction

When compared with metal and ceramic based traditional engineering materials, carbon fibers exhibit low density and superior mechanical properties in terms of high strength and high stiffness [1]. Due to their desirable properties, carbon fibers are extensively used in the manufacturing of military and civilian aeroplanes as a reinforcement material for the production of primary and secondary structural composites, in wind turbines for the production of clean and renewable energy, in the civilian construction projects, pressure tanks in automotive industry, off-shore tethers for the deep-sea oil platforms, medical and sporting goods etc. [2,3].

Edison in 1880 produced the first cellulose based carbon fiber to be used as a light-bulb filament [4]. Since then considerable research and development efforts were made to produce carbon fibers with desirable properties in the 1950s and 1960s by researchers in England [5], USA [6] and Japan [7].

The earliest commercially available carbon fibers were produced from regenerated cellulose precursors available in the form of continuous filament bundles. Later studies were directed towards the commercially available polyacrylonitrile (PAN) precursor. Watt and Johnson at Royal Aircarft Establishment in England [5] and Shindo at the Government Industrial Research Institute in Japan [6] developed procedures to produce carbon fibers from PAN. Although earlier investigators used cellulose as a precursor for carbon fiber production, nowadays, majority of carbon fibers are produced from PAN precursor followed by petroleum pitch.

In terms of annual worldwide production, almost 90 % of the carbon fiber is produced from PAN precursor, followed by petroleum pitch and cellulose precursors. According to a recently published report [9], 34,200 metric tons of carbon fiber consumption was estimated for the year ending 2010. The main carbon fiber producers are located in Japan (Toray Industries, Toho Tenax, Mitsubishi Rayon, Mitsibushi Chemical, Nippon Graphite), Hungary (Zoltek), Taiwan (Formosa Plastics), Germany (SGL Carbon), and USA (Hexcel and Cytec Engineered Materials) [9]. Due to low tensile strength, low elastic modulus and low carbon yield characteristics, cellulose based carbon fibers are not used for high-strength applications in favor of PAN and pitch based carbon fibers. Cellulose precursors are nowadays utilized for the manufacturing of activated carbon fibers [10]. Activated carbon fibers are used for the production of gas storage, nuclear-biological and chemical (NBC) protective suits and for environmental pollution control purposes [10].

Theoretically speaking, it should be possible to produce carbon fibers with an elastic modulus of 1000 GPa and a tensile strength of 100 GPa [11]. Unfortunately, due to the presence of structural defects such as surface flaws, experimental values of tensile strength and elastic modulus never reached the theoretical ones. Due to the very high molecular orientation introduced during the processing of mesophase pitch fibers, it is now possible to produce carbon fibers with an elastic moduli approaching to that of theoretical value. Cytec Industries of USA produced mesophase pitch based carbon fiber introduced under the trade name Thornel K-1100 with an elastic modulus of 965 GPa [12], almost

*Corresponding author: ismailkaracan@erciyes.edu.tr

97 % of the theoretical value. Unfortunately, due to very high manufacturing costs of mesophase pitch based carbon fibers in comparison with PAN-based carbon fiber production, the annual production rate of pitch based carbon fibers is achieved to be below 1000 tons [9].

There is now a growing interest in producing carbon fibers using alternative precursors. Several attempts were made to use aliphatic linear chain polymer fibers for the production of carbon fiber. Polyethylene [13-15], polypropylene [16], polyvinyl alcohol [17-19], polystyrene [20], syndiotactic 1,2-polybutadiene [21] and polyvinylidene chloride/vinyl chloride copolymer fibers [22] were reported to be utilized for the production of carbon fibers going through the thermal stabilization and carbonization stages.

Fully aromatic fibers with high thermal stability were considered by several investigators for the production of carbon fibers. The idea behind using the aromatic fibers was to avoid thermal stabilization stage normally applied for the fibers with low thermal stability and with low melting temperatures. Direct carbonization is only needed to produce carbon fibers from such aromatic precursors. Poly(p-phenylene terephthalamide) fiber produced by Du Pont under the trade name Kevlar® with a high thermal stability was used for producing carbon fiber through a one or two-step direct carbonization [23], which was intended to be used as an anode material in lithium secondary batteries. Poly(p-phenylenebenzobisoxazole) (PBO) commercially produced by Toyobo Company of Japan under the trade name of Zylon® was also reported to be used to produce carbon fiber without going through the thermal stabilization stage [24]. Poly(meta-phenylene terephthalamide) fiber produced by Du Pont under the trade name Nomex® was utilized to produce activated carbon fiber by going through the direct carbonization stage followed by activation with carbon dioxide [25]. Polyoxadiazole (POD) [26], phenol hexamine [27], polybenzimidazole (PBI) [28] fibers were another examples of highly aromatic precursors to produce carbon fiber going through direct carbonization stage without going through thermal stabilization.

Apart from aromatic polyamides [23,25], aliphatic polyamides such as polyamide 6 or polyamide 66 precursor fibers were the subject of a few investigations of producing carbon fibers [29-32]. Unlike aromatic polyamides, aliphatic polyamides such as polyamide 6 (PA6) or 6.6 need to go through the thermal stabilization prior to carbonization process. Thermal stabilization of PA6 was obtained by sulfonation using 2,5-dichloro-benzenesulfonyl chloride (DBSC) [33]. With this treatment, no melting was reported to occur at up to 1000 °C. Electron beam induced crosslinking of PA6 in the presence of triallyl cyanurate (TAC) lead to increased thermal stability [34]. Hindered phenolic antioxidant system incorporated in the melt of PA6 also showed thermal stabilization effect [35].

Several alkali and transition metal salts were reported to be capable of forming coordination complexes with the amide groups of polyamides [36-43]. These complexes not only improve thermal stability [36,37] but also cause major changes in glass transition temperature [38], melting point, crystallinity [39,40], stress cracking [41], mechanical properties [42] and conductivity [43].

During the course of the present investigtion, melt-extruded polyamide 6 fiber is suggested as a low cost alternative precursor for the production of carbon fiber, due to its relatively good carbon content (theoretical carbon content of 63.7 %), ready availability, low cost, recyclability and easy processability. According to the latest published figures [44], the latest polyamide fiber production in 2009 stood at 3.5 million tons per annum for filaments and staple fibers. This figure is considered to be much higher than the annual production rate of polyacrylonitrile fibers. By the end of 2009, acrylic production of filaments and staples stood at 1.9 million tons per annum [44].

The aim of the present investigation was to study the role of cupric chloride pretreatment on the thermal stabilization of polyamide 6 fibers prior to carbonization stage. The structural characterization was carried out using a combination of X-ray diffraction and thermal analysis (DSC and TGA) measurements with the aim of monitoring and following the structural transformations as a function of stabilization time.

Experimental Details

Preperation of Thermally Stabilized Samples

Untreated polyamide 6 (PA6) precursor multifilament bundle as a textile grade was obtained from SIFAS AS (Bursa, Turkey). PA6 was provided with a linear density of 8.53 tex per 68 filaments. Untreated PA6 multifilament bundle was treated with 5 % (v/v) aqueous ethanol solution for 30 mins at 50 °C to remove the spin finish oil present on the surface of the fibers followed by a thorough washing under running water for 30 mins to remove the final remains. Chemical treatment was carried out by immersing the samples in 4.44 % (w/v) aqueous cupric chloride dihydrate solution at 95 °C for 2 h. This concentration is equal to 3.5 % (w/v) cupric chloride anhydrous, which is the dry weight of cupric chloride without two water molecules. Cupric chloride dihydrate was obtained from Kimetsan AS (Ankara, Turkey) with a purity of 99 %.

Thermal stabilization was subsequently carried out in a circulating air atmosphere at an isothermal temperature of 180 °C for stabilization times ranging from 0.25 to 24 h. The samples were originally wound onto stainless steel frames with the aim of constraining the samples to prevent physical shrinkage and also to prevent the loss of molecular orientation. Thermal stabilization was carried out with a heating rate of 1 °C/min.

Experimental Data Collection

Evaluation of Fiber Diameter

Diamater of the untreated, cupric chloride pretreated and thermally stabilized PA6 fibers was evaluated using a polarizing microscope (Nikon ME600L, Japan) with a calibrated eyepiece. 20 readings along the fiber axis direction of at least 5 different filaments were used during the fiber diameter measurements.

Evaluation of Linear Density

Linear density was determined by measuring the weight in grams per unit length of a multifilament bundle. In the present investigation, tex is used as a linear density which is defined as the weight of a multifilament bundle in grams per 1000 meters.

Evaluation of Burning Test

Samples were exposed to a match flame to see whether they burn or not. The results are assessed simply as pass or failure.

X-ray Diffraction

The wide-angle X-ray diffraction traces were obtained using a Bruker® AXS D8 Advance X-ray diffractometer system utilizing nickel filtered CuK_{α} radiation (wavelength of 0.154056 nm) and voltage and current settings of 40 kV and 40 mA, respectively. Counting was carried out at 10 steps per degree. The observed equatorial X-ray scattering data was collected in reflection mode in the 10-35° 2θ range.

Thermal Analysis

Differantial Scanning Calorimetry

The differential scanning calorimetry (DSC) experiments were carried out using a Perkin Elmer Diamond DSC system. Typical sample weights used were approximately 5 mg. The heating rate of 10 °C/min and an upper temperature range of 350 °C were selected. Indium (m.p. 156.6 °C and ΔH = 28.45 J/g,) was used for heat flow calibration. Indium and zinc (m.p. 419.51 °C) standards were used for temperature calibration. The specimens were always tested under a nitrogen flow rate of 50 ml/min.

Thermogravimetric Analysis

Thermogravimetric Analysis (TGA) thermograms were collected using a Perkin Elmer Diamond Thermogravimetric/ Differential Thermal Analyzer. Typical sample weights used in the measurements were approximately 4-6 mg. The heating rate of 10 °C/min and an upper temperature range of 1150 °C were selected. The temperature calibration of TG/ DTA was carried out using the melting points of indium (m.p. 156.6 °C), tin (m.p. 231.88 °C), zinc (419.51 °C), aluminium (m.p. 660.1 °C) and gold (m.p. 1064.18 °C) standards. The weight balance calibration was performed by using a standard weight of 20 mg at room temperature in both systems. Experiments were performed under a nitrogen flow of 200 ml/min. Data from TGA was used in the evaluation of weight loss and % char yield for the untreated and the cupric chloride pretreated-thermally stabilized PA6 fiber samples.

Experimental Data Analysis

Evaluation of DSC Crystallinity from Melting Enthalpy Values [45]

Assuming a two-phase model consisting of crystalline and amorphous phases, the degree of DSC crystallinity can be evaluated from the melting enthalpies using equation (1)

$$\chi_c = \frac{\Delta H_m}{\Delta H_m^o} \times 100\ \% \tag{1}$$

where χ_c is the degree of crystallinity evaluated by DSC method, ΔH_m is the melting enthalpy of the sample and ΔH_m^o is the melting enthalpy of 100 % crystalline sample and an intermediate value of 190 J/g was taken for 100 % crystalline PA6 [46].

Evaluation of Conversion Index from Differential Scanning Calorimetry [47]

DSC based conversion index is evaluated using equation (2).

$$\text{DSC - Conversion index (\%)} = \frac{\Delta H_o - \Delta H}{\Delta H_o} \times 100\ \% \tag{2}$$

Where ΔH_o is the melting enthalpy of untreated PA6 fiber and, ΔH is the melting enthalpy of cupric chloride pretreated and thermally stabilized PA6 fiber, respectively.

X-ray Data-curve Fitting

All the X-ray diffraction traces obtained from the untreated and cupric chloride pretreated and thermally stabilized PA6 fiber samples were fitted with a curve fitting procedure developed by Hindeleh *et al*. [48] to separate the overlapping peaks. Each profile is considered to have the combination of Gaussian and Cauchy functions. When the observed and calculated intensity traces converge to the best acceptable parameters, the computer program provides the list of accurate peak parameters in terms of profile function parameter (f), peak height, peak width at half height and peak position.

Curve fitting of equatorial X-ray diffraction traces was carried out with three crystalline and one amorphous peak together with a linear baseline. The region below the baseline is attributed to instrumental background signal which may include air and incoherent scattering. The peak height of the amorphous contribution was adjusted in such as way that the tail regions fitted very well with the experimental data points. The peak position and half-height width of the

amorphous phase was also allowed to vary. During the curve fitting stage, the peak position of the amorphous phase was found to vary between 20.9 and 22.3 º, in agreement with the published literature [49].

Evaluation of Apparent X-ray Crystallinity

Apparent X-ray crystallinity is based on the ratio of the integrated intensity under the resolved peaks to the integrated intensity of the total scatter under the experimental trace [50]. This definition can be expressed as in the equation (3)

$$\chi_c = \frac{\int_0^{\infty} \mathbf{I}_{cr}(2\theta)d(2\theta)}{\int_0^{\infty} \mathbf{I}_{tot}(2\theta)d(2\theta)} \quad (3)$$

It should be emphasized that the apparent X-ray crystallinity was defined between two arbitrarily chosen angles and should be considered to be an optimum mathematical solution. In this work, the apparent X-ray crystallinity was estimated in the 2θ range between 10 and 35 º.

Evaluation of X-ray Conversion Index

X-ray conversion index is determined using equation (4)

$$\text{X-ray - conversion index} = \frac{\Sigma I_o - \Sigma I}{\Sigma I_o} \times 100\ \% \quad (4)$$

Where $\Sigma I_o = \mathbf{I}_{\alpha(200)} + \mathbf{I}_{\gamma(200)} + \mathbf{I}_{\alpha(002)}$ is the sum of the intensities of the $\alpha(200)$, $\gamma(200)$ and $\alpha(002)$ reflections from the untreated PA6 fiber and $\Sigma I = \mathbf{I}_{\alpha(200)} + \mathbf{I}_{\gamma(200)} + \mathbf{I}_{\alpha(002)}$ is the sum of the intensities of the $\alpha(200)$, $\gamma(200)$ and $\alpha(002)$ reflections from the cupric chloride pretreated and thermally stabilized PA6 fiber, respectively. The values of the intensities are obtained after the curve fitting procedure.

Results and Discussion

Cupric chloride ($CuCl_2$) pretreated PA6 fibers were subjected to thermal stabilization treatment in a circulated air environment at an isothermal temperature of 180 ºC for various lengths of time ranging from 0.25 to 24 h (Table 1).

Thermal stabilization resulted in the change of the color of the samples from white, through shades of yellow, brown, dark brown in the early stages to blackish and black in the final stages (Table 1). Color changes during the thermal treatment of PA6 fibers may be partly due to the dehydration of the hydrated cupric chloride. The change to the deep colors of the samples in the advanced stages should be regarded as an evidence for the presence of thermally stabilized structure.

The results of the burning tests are given in Table 1. The samples passed the critical burning test after about 8 h of thermal treatment, which showed that the samples thermally treated for 8 h and beyond were properly stabilized and ready for the carbonization stage (Table 1).

The change of fiber diameter of stabilized samples as a function of stabilization time is presented in Table 1. The diameter of the stabilized samples with treatment time of 24 h was reduced from 12 μm to 10.4 μm. The fibre diameter fell off sharply after an initial stabilization time of 0.5 an hour and further falls continued with progressing stabilization time. The most severe reduction in fiber diameter was observed after 24 h of stabilization time with approx. 13 % loss in fiber diameter (Table 1) occurred with respect to the thermally untreated sample. The main reason for the decrease in fiber diameter is most likely due to the weight loss occurred during the oxidative thermal stabilization stage.

The linear density of the untreated PA6 fiber was found to be increased by 27 % following the cupric chloride pretreatment prior to thermal treatment. The variation of the linear density of the thermally stabilized PA6 multifilament bundle is presented in Table 1 as a function of stabilization time. Linear density decreased by 13 % after 1/4 of an hour of stabilization time followed by a continuous and steady decline with progressing time. Linear density loss continued

Table 1. Characteristics of thermally stabilized polyamide 6 fibers

Stabilization time (hour)	Color change	Burning test	Fiber diameter* (μm)	Fiber diameter variation (%)	Linear density (Tex)	Linear density variation (%)
0	White	Fail	12.0 (0.4)	0.0	10.85	0
0.25	Yellow	Fail	11.8 (0.4)	-1.6	9.42	-13.2
0.5	Dark Yellow	Fail	11.5 (0.4)	-4.3	9.30	-14.3
1	Light Brown	Fail	11.4 (0.5)	-4.7	9.26	-14.7
2	Brown	Fail	11.4 (0.4)	-5.2	9.03	-16.3
4	Dark Brown	Fail	11.3 (0.4)	-6.1	8.76	-19.3
6	Blackish	Fail	10.8 (0.4)	-9.8	8.57	-21.0
8	Black	Pass	10.7 (0.4)	-10.6	8.14	-25.0
10	Black	Pass	10.6 (0.5)	-11.5	8.11	-25.3
12	Black	Pass	10.6 (0.5)	-12.1	8.00	-26.3
24	Black	Pass	10.4 (0.4)	-13.0	7.29	-32.8

Values in parantheses are given as standard deviations.

up to the stabilization time of 24 h for the cupric chloride pretreated and thermally stabilized PA6 fibers. Linear density loss of 33 % with respect to cupric chloride pretreated sample without thermal stabilization occurred after 24 h.

The linear density loss with progressing time is likely to be due to the possible loss of elementary carbon, hydrogen, nitrogen and oxygen during the thermal stabilization process. However, cupric ions are not expected to be lost during the thermal stabilization due to its high melting and volatilization temperature.

Differential Scanning Calorimetry

DSC scans of the untreated and cupric chloride pretreated and thermally stabilized PA6 fibers are shown in Figure 1. All the thermograms shown in Figure 1 showed a minor endotherm due to the dehydration of adsorbed water in the 40-120 ºC region followed by a melting endotherm. Table 2 shows that the incorporation of cupric ions into PA6 fibers caused depression of the melting temperature of about 27 °C. As shown in Table 2, melting points droped from 220 °C for the untreated sample to 193 °C for the cupric chloride pretreated and thermally stabilized sample for 1/4 of an hour. Thereafter, there was a gradual but monotonous increase to 198 °Cafter 24 hours of stabilization time.

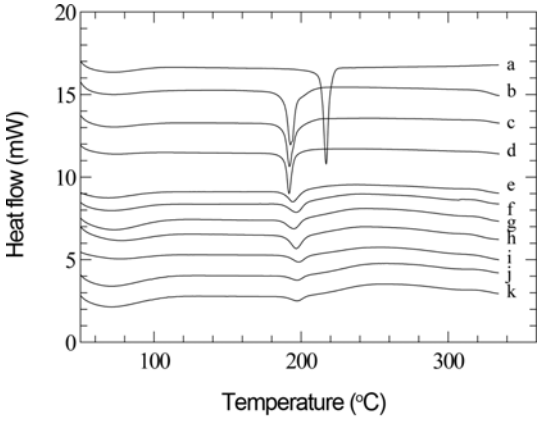

Figure 1. DSC thermograms of untreated (a) and cupric chloride pretreated and thermally stabilized PA6 fibers as a function of stabilization time. (b) 180 ºC 0.25 h, (c) 180 ºC 0.5 h, (d) 180 ºC 1 h, (e) 180 ºC 2 h, (f) 180 ºC 4 h, (g) 180 ºC 6h, (h) 180 ºC 8 h, (i) 180ºC 10 h, (j) 180 ºC 12 h, (k) 180 ºC 24 h.

Table 2. Thermal characteristics of unstabilized and thermally stabilized polyamide 6 fibers

Stabilization time (hour)	Melting peak (°C)	Melting enthalpy ΔH (J/g)	DSC crystallinity (%)	DSC-conversion index (%)
0	220.0	54.9	28.9	0.0
0.25	193.0	51.6	28.2	6.0
0.5	192.0	45.1	27.2	17.9
1	192.0	35.8	23.7	34.8
2	194.5	17.8	18.8	67.6
4	197.0	11.3	9.4	79.4
6	196.0	8.1	5.9	85.3
8	196.7	7.1	4.3	87.1
10	197.6	6.7	3.7	87.8
12	197.9	5.0	3.5	90.9
24	198.2	3.2	2.6	94.2

It has been reported that the incorporation of metal halides ($CuCl_2$, $CuBr_2$, $FeCl_3$) into PA6 cause melting point depressions and a strong retardation of crystallization rate [39]. The depression in melting point is reported to be stronger in copper halides than the iron halide [39]. Glass transition (T_g) temperature of PA6 upon incorporation of cupric chloride was reported to increase with increasing cupric ion content but the rate of increase in T_g was reported to be lower for the cupric chloride system than for the ferric chloride [38] with identical metal halide content. A definitive conclusion about this point could be drawn only after thermal treatment of untreated PA6 is carried out.

Dunn and Sansom [41], investigated the stress characteristics of polyamides using various inorganic salts, and reported that the salts may be classified into two types. In type I metal halides (Zn, Co, Cu, Fe, Cr, and Mn chloride), the metal atoms form metal complexes by coordination bonding with the carbonyl oxygen of the amide group while in type II metals (Li, Ca and Mg chloride), the halogen atoms of the salt form complex with N-H replacing the N-H-O hydrogen bond. The salt (cupric chloride) used in the present investigation belongs to type I category. Type I metal halides are reported to cause stress cracking by interference with the hydrogen bonding of the polyamide structure. The metal halides belong to the type II inorganic salts are reported to cause solvent cracking.

It is highly likely that Cu^{2+} ions will coordinate with the carbonyl oxygen of the amide groups. The coordination of cupric ions is expected to break the hydrogen bonds between PA6 chains. Since the cupric ions form complex bonds with the carbonyl (C=O) groups, N-H bonds are left free without hydrogen bonding. The perturbation of the hydrogen bonds is one of the reasons for the lowering of the melting temperature following the cupric chloride pretreatment.

Complexation of cupric ions with the amide groups is likely to take place primarily in the amorphous regions due to relatively easy diffusion of cupric ions into such regions. In the advanced stages of stabilization, complexation is expected to progress into the ordered regions following the destruction of hydrogen bonds due to complexation of cupric ions with the amide groups together with the added influence and contribution of thermal energy.

With progressing stabilization time at 180 ºC, it can be seen in Table 2 that the melting enthalpy (ΔH) values decrease as a result of decrystallization effects. The melting

enthalpy values can be used to assess the degree of crystallinity. The structure of PA6 fiber exhibits a polymorphic crystal character and contains a mixture of more stable α-phase and a less stable γ-phase [51]. The γ-phase is reported to be stable up to a temperature of 170 ºC and gets converted to the more stable α-phase at higher temperatures [52]. This suggests that the melting enthalpy measured above 170 ºC and beyond in the DSC thermograms shown in Table 2 corresponds to almost α-phase. DSC-crystallinity (%) values evaluated using equation (1) listed in Table 2 decrease as a result of decrystallization effect (i.e. amorphization) with stabilization time. DSC-crystallinity was found to decrease from 29 % for the untreated sample to 3 % for the cupric chloride pretreated and thermally stabilized sample after 24 h of stabilization time. The melting point reduction and the decrystallization effects are due to the direct consequence of strong binding between the cupric ions (Cu^{2+}) and the amide bonds of PA6 fibers [39].

DSC was also used for the determination of conversion index using equation (2). Figure 1 shows the near disappearance of melting endotherm after 24 h of stabilization time. An almost complete disapperance of the melting entotherm suggests that the samples stabilized for 24 h indicate nearing the completion of the cyclization reactions for the present investigation. Cyclization of PA6 chains is possibly aided by the complexation of cupric ions with the amide groups forming rings containing 5 or 6 atoms resistant to high temperatures. Further carbonization under inert atmosphere is expected to form aromatized structures containing extensive intermolecular crosslinks leading to the formation of graphitic structures. DSC-conversion index continously increases until 24 h of stabilization time and shows variation between 6 and 94 % for the samples stabilized for 1/4 and 24 h, respectively (Table 2).

Thermogravimetric Analysis

Thermogravimetric analysis technique was used for the characterization of thermal stability of untreated, cupric chloride pretreated and thermally stabilized PA6 fibers. Experience in our laboratory shows that relatively steeper and narrower temperature range related weight losses reflects faster decomposition reactions and results in considerable weight losses which in turn results in lower char yields.

Untreated PA6 (Figure 2(a)) sample remains stable from 50 to 300 °C, where there is no visible sign of weight loss. This zone of thermal stability is followed by a relatively faster rate of decomposition up to 480 °C. Total weight loss around 1000 °C for this sample reaches 98 % with a resulting char yield of 2 %. TGA thermograms of cupric chloride pretreated and thermally stabilized PA6 fibers (Figure 2(b)-(i)) showed the loss of absorbed moisture up to 110 °C and a much faster weight loss was observed in the temperature region between 300 and 480 °C due to catalytical effect of cupric ions involved in the radical degradation reactions of PA6 fiber.

TGA thermograms of cupric chloride pretreated and thermally stabilized PA6 fibers are plotted in Figure 2 as a function of stabilization time. TGA thermograms show decreasing weight loss with increasing stabilization time indicating increasing char yield due to the increasing crosslinking density between PA6 polymer chains. Untreated sample loses weight over a narrow temperature range whereas thermally stabilized samples lose weight over a wider temperature range due to the increased crosslinking related ladder-like structure formation.

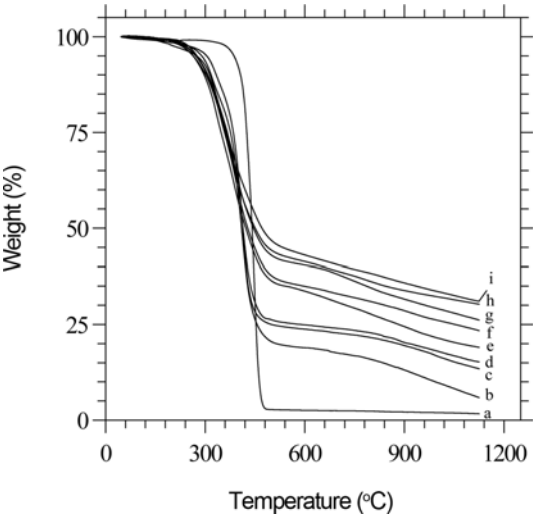

Figure 2. TGA thermograms of untreated (a) and cupric chloride pretreated and thermally stabilized PA6 fibers as a function of stabilization time. (b) 180 ºC 0.25 h, (c) 180 ºC 0.5 h, (d) 180 ºC 1 h, (e) 180 ºC 2 h, (f) 180 ºC 4 h, (g) 180 ºC 6 h, (h) 180 ºC 8 h, (i) 180 ºC 10 h, (j) 180 ºC 12 h.

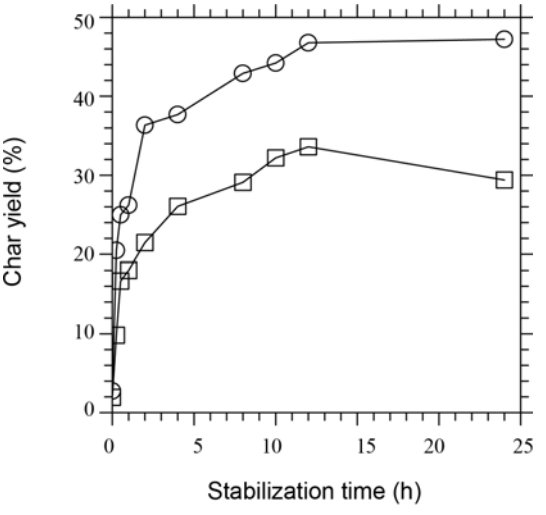

Figure 3. Comparison of char yield values of untreated and cupric chloride pretreated and thermally stabilised PA6 fibers at different temperatures; (○) 500 °C and (□) 1000 °C.

Figure 3 shows the comparison of the char yields at 500 and 1000 °C obtained from the untreated and cupric chloride pretreated and thermally stabilized PA6 fibers. The results show an increasing char yield with increasing stabilization time. Char yield reaches maximum value of 33.6 % at 1000 °C for the cupric chloride pretreated PA6 fibers stabilized for 12 h at 180 °C. Due to a slight weight loss at the stabilization time of 24 h, TGA thermogram of the cupric chloride pretreated-thermally stabilized PA6 fiber stabilized at 24 h is not placed in Figure 2.

The results obtained from the TGA analysis show that the cupric chloride pretreated-thermally stabilized PA6 fibers acquire higher thermal stability than the untreated PA6 fiber as a result of the oxidation based crosslinking reactions. Cupric chloride pretreatment seems to result in a much more efficient thermal stabilization and carbonization (during the simulated carbonization of TGA runs under nitrogen atmosphere) reactions, possibly due to the more efficient cyclization and intermolecular crosslinking reactions. Cupric chloride pretreatment resulted in an efficient cyclization and dehydrogenation reactions. Unsaturated sites created by the loss of hydrogen atoms during the dehydrogenation process then progressed with the formation of intermolecular crosslinks and resulted in a high char yield content. It seems that cupric chloride promoted coordination bonds between carbonyl oxygen of the amide groups and cupric ions which encouraged the formation of intramolecular reactions.

The results suggest the strong interaction between cupric ions and the amide groups of PA6 fiber during the thermal stabilization stage and led to the formation of intramolecular and intermolecular crosslinks which caused the formation of large amount of carbonized structure in an inert atmosphere.

X-ray Diffraction

Polyamide 6 structure exhibits a polymorphic crystal character and exists in several crystal forms, the most important of which are the α and the γ-crystal phases. Both crystal phases have monoclinic unit cell structure with different directions of hydrogen bonds between adjacent chains [51]. Both crystalline structures possess monoclinic unit cells assuming b-axis as the unique axis, parallel to the chain axis (along the fiber axis direction) [53].

It has been demonstrated that the shifting of the hydrogen bonds generates different crystalline forms. α-phase is characterized by a stable monoclinic crystal structure consisting of fully extended planar zig-zag chains, where adjacent antiparallel chains are linked to each other by hydrogen bonds within (002) planes [54]. In the γ-phase, molecular chains have to twist away from the planar zig-zag chains to form hydrogen bonds between parallel chains within (200) planes consisting of up and down chain displacements. Such twisting of chains results in the shortening of the crystallographic chain axis dimension. As a result, the crystalline density of γ-phase is smaller than that of α-phase [55].

As a result of twisting of amide groups with respect to the methylene groups, the distance between the amide groups is expected to be longer for the γ-phase than that of the α-phase. This behavior of hydrogen bonding in γ-form is likely to lead to lower interchain interactions than that of the α-form. It has been reported that α-phase is most commonly observed at room temperature and can be converted to γ-phase with a pretreatment of iodine-potassium iodide solution followed by removal of the absorbed iodine by water, acetone, ethylenediamine [56] or sodium thiosulphate [57].

High speed extrusion of PA6 filaments also favors the formation of γ-phase [58-60]. Different crystalline structures of α and γ-phases are known to impart different physical and mechanical properties. Elastic modulus of α-phase is reported to be higher than that of γ-phase [61]. The strength of hydrogen bond is reported to be higher in the α-crystalline phase than that of the case with γ-phase. Due to difference in the crystalline structures, the density of the α-crystalline phase of 1.23 g/cm^3 is significantly higher than that of the γ-phase. The density of γ-phase is about 1.17 g/cm^3 [55].

Figure 4 shows the equatorial X-ray diffraction traces of untreated and cupric chloride pretreated PA6 fiber thermally stabilized at 180 ºC as a function of stabilization time. X-ray diffraction traces shown in Figure 4 are displaced along the ordinate (Y-axis) for clarity. X-ray diffraction traces presented in Figure 4 do not show any evidence for the presence of diffraction peaks due to the incorporated cupric chloride species. Also, the incorporation of cupric chloride did not seem to modify the typical equatorial X-ray diffraction traces, which included the characteristic reflections of both the α and γ-phases. This indicates that cupric chloride did not seem to diffuse into the crystalline regions and seem to be present only in the disordered regions.

Curve fitted equatorial X-ray diffraction trace of untreated PA6 fiber presented in Figure 5 shows the presence and

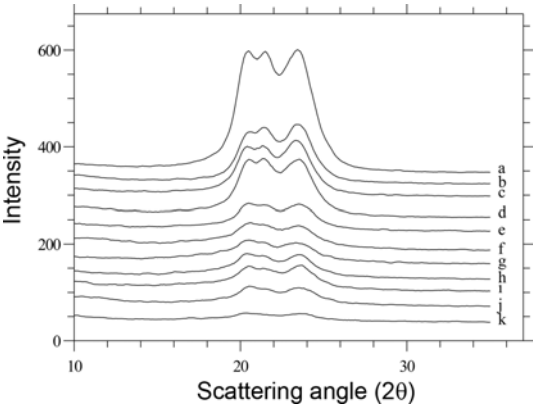

Figure 4. Equatorial X-ray diffraction traces of untreated (a) and cupric chloride pretreated PA6 fibers thermally stabilized at 180 °C as a function of stabilization time; (b) 180 °C 0.25 h; (c) 180 °C 0.5 h; (d) 180 °C 1 h; (e) 180 °C 2 h; (f) 180 °C 4 h; (g) 180 °C 6 h; (h) 180 °C 8 h; (i) 180 °C 10 h; (j) 180 °C 12 h; (k) 180 °C 24 h.

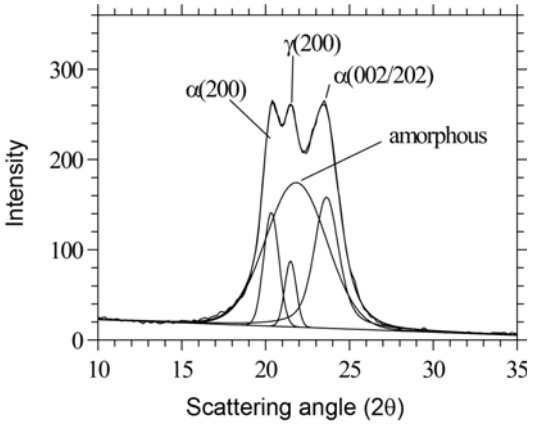

Figure 5. Curve fitting of equatorial X-ray diffraction trace of untreated PA6 fiber.

coexistence of a polymorphic structure containing α and γ-crystalline forms along with an amorphous phase.

Qualitative inspection of the equatorial X-ray diffraction trace of PA6 fiber shows three strong well-defined reflections with d-spacings of 0.436, 0.413 and 0.378 nm which can be indexed as the α-form (200), γ-form (200) and α-form (002/202) reflections (Figure 5).

Cupric chloride pretreatment and the following thermal stabilization in air at an isothermal temperature of 180 °C appeared to have a significant impact on the molecular structure. The qualitative inspection of equatorial X-ray diffraction traces (Figure 4) pointed to the loss of the apparent crystallinity in terms of the loss of lateral order with progressing time.

Equatorial X-ray diffraction traces presented in Figure 4 showed the variation of the peak heights corresponding to α-phase (200), γ-phase (200) and α-phase (002/202) reflections as a function of stabilization time. Hydrogen bonding of α-phase occurs within the (002) planes whereas in the γ-phase takes place within the (200) planes. The results suggested the loss of hydrogen bonds with progressing time due to the loss of the intensity of α-phase (002/202) and γ-phase (200) reflections (Figure 4).

It appears that a typical decrystallization (i.e. amorphization) process caused by the loss of hydrogen bonds was taken place during the thermal stabilization stage with progressing time. Figure 6 shows that the α-phase (200) and (002/202) reflections show higher intensity values than that the γ-phase (200) reflection. It indicates that α-phase may exhibit higher crystalline orientation than that of the γ-phase. Vasanthan [62] using X-ray diffraction analysis of PA6 fibers drawn up to the draw ratio of 4 showed that α-phase crystalline orientation was always higher than that of γ-phase crystalline structure. The orientation of both phases increased with increasing draw ratio [62].

Peak parameters obtained from the curve fitting of the equatorial X-ray diffraction traces can be used to obtain the

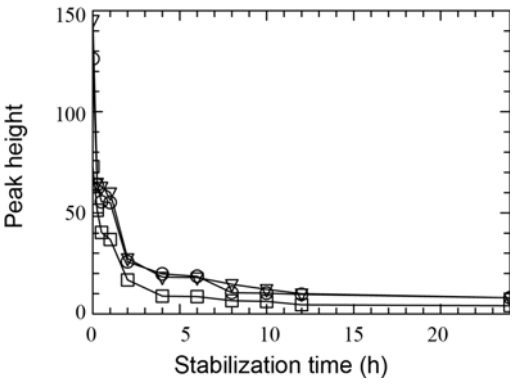

Figure 6. Comparison of the intensity of α(200), γ(200) and α(002/202) reflections of untreated and cupric chloride pretreated and thermally stabilized PA6 fiber as a function of stabilization time. (▽) α-phase (002/202) peak, (○) α-phase (200) peak, and (□) γ-phase (200) peak.

Table 3. X-ray diffraction analysis of cupric chloride pretreated and thermally stabilized PA6 fibers as a function of stabilization time

Stabilization time (hour)	α-phase fraction (%)	γ-phase fraction (%)	Amorphous fraction (%)	X-ray conversion index (%)
0	28.8	3.9	67.3	0
0.25	20.5	3.8	75.7	47.8
0.5	19.1	3.6	77.3	54.0
1	16.7	3.5	79.8	55.9
2	16.6	3.4	80.0	80.7
4	16.2	3.3	80.5	86.4
6	15.5	2.9	81.6	86.9
8	9.8	2.4	87.8	90.8
10	9.3	2.0	88.7	91.7
12	9.3	1.9	88.8	93.0
24	6.4	0.9	92.7	94.2

fractions of the crystal forms and the degree of apparent crystallinity. Resolved peak areas were used for the evaluation of the phase fractions according to equation (3). α-phase fraction was evaluated using the total peak areas of (200) and (002/202) reflections whereas the fraction of γ-phase was evaluated using only the peak area of (200) reflection. Table 3 shows the comparison of the phase fractions in terms of α, γ and amorphous phases as a function of stabilization time. Table 3 shows that the fraction of the α-phase is always higher than that of the γ-phase and the fraction of both phases decrease with progressing time. Whereas, the amorphous phase fraction continuously increased with time due to the onset and the progress of amorphization process taking place during the stabilization stage. α-phase fraction decreased from 29 to 6 % after 24 h, whereas γ-phase decreased from 4 to 1 % after 24 h of stabilization

time. On the other hand, amorphous phase fraction increased from 67 to 93 % after 24 h of stabilization.

A novel approach was developed for the determination of X-ray conversion index using the intensities of $\alpha(200)$, $\gamma(200)$ and $\alpha(002)$ reflections obtained from the curve fitting procedure using equation (4). The results presented in Table 3 showed the increasing values of X-ray conversion index with progressing time which can be considered to be a reliable method to estimate the proportion of ladder structure formed during the stabilization process. The results listed in Table 3 showed a rapid stabilization only after 1/4 of an hour of stabilization time reaching a value of 48 %. The value of the X-ray conversion index for the sample stabilized for 24 h was 94 %.

Incorporation of cupric ions into the polymer structure via complexation with the amide groups along the polymer chain direction is likely to assist the formation of ladder-like network structure leading to increased X-ray conversion index with progressing time. The formation of complexation between cupric ions and amide groups is also the main reason behind the decrystallization process as a result of the loss of hydrogen bonds during the stabilization stage. Supporting evidence comes from the published data of Siegmann and Baraam [39] who showed the incorporation of cupric chloride caused a strong retardation of the crystallization rate of PA6. Similar findings were also observed with the incorporation of ferric ions [63].

DSC and X-ray conversion indices are plotted and compared in Figure 7. The results presented in Figure 7 showed that the ladder-like structure formation was accelerated within the first 1 hour of the stabilization process. DSC-conversion index laged behind in the early stages of stabilization time but catched up during the advanced stages. X-ray conversion index showed an almost full stabilization after 2 hours of stabilization time whereas DSC stabilization index showed an underestimated stabilization under the same conditions. Both conversion indices converged after 6 hours of stabilization time and increased steadily and monotonously until the stabilization time of 24 h. After 24 hours of stabilization time, X-ray and DSC conversion indices converged to the value of 94 %.

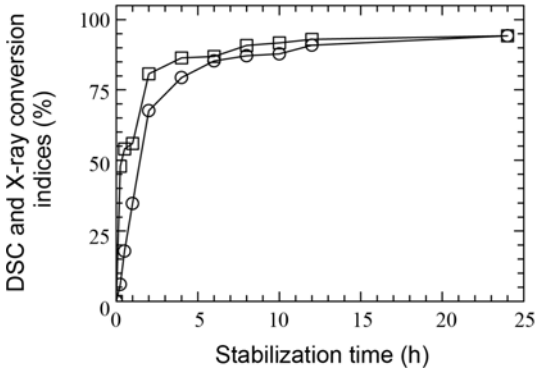

Figure 7. Comparison of DSC and X-ray conversion indices of untreated and cupric chloride pretreated PA6 fibers thermally stabilized at 180 °C as a function of stabilization time; (□) X-ray conversion index and (○) DSC conversion index.

Conclusion

The influence of cupric (Cu^{2+}) ion incorporation during the thermal stabilization of polyamide 6 precursor fibers was investigated using a combination of differential scanning calorimetry (DSC), thermogravimetric analysis (TGA) and X-ray diffraction measurements. The results obtained from cupric chloride pretreated and thermally stabilized PA6 fibers showed the reduction in fiber diameter and linear density values with increasing stabilization time. Thermally stabilized PA6 samples also exhibited color changes from light brown to black with progressing time. PA6 fibers were found to be properly stabilized after 8 h of stabilization time. The results obtained from DSC and TGA measurements clearly indicated an improvement in the thermal stability when cupric (Cu^{2+}) ions were incorporated into the polymer structure. Cupric chloride pretreatment followed by thermal stabilization resulted in a highly cross-linked structure which is expected to withstand the high temperatures involved during the carbonization stage. TGA thermograms showed that thermal stability was improved as indicated by increasing char yield with progressing time. Char yield reached a value of 33.6 % at 1000 °C for the cupric chloride pretreated PA6 fibers thermally stabilized for 12 h at 180 °C. The results obtained from DSC and X-ray diffraction methods showed the effect of decrystallization as a result of disruption of hydrogen bonds. It was found that cupric ion-amide coordination bond formation improved the thermal stabilization by aiding the development of ladder-like structures. The investigation resulted in a new method of evaluation of X-ray stabilization index specifically for the thermally stabilized PA6 fiber.

Acknowledgements

The assistance and cooperation of SİFAŞ AŞ (Bursa) is gratefuly acknowledged for providing the polyamide 6 multifilaments. The financial support of the Scientific Research Projects Unit of Erciyes University is very much appreciated (project number FBA-09-955). Thanks are also extended to an anonymous reviewer for useful comments.

References

1. J. B. Donnet and R. C. Bansal, “Carbon Fibers”, Marcel Dekker, New York, 1984.
2. P. D. Mangalgiri, *Bull. Mater. Sci.*, **22**, 657 (1999).
3. D. L. Chung, “Carbon Fiber Composites”, pp.3-65, Butterworth-Heinemann: Boston, M.A., USA, 1994.
4. T. A. Edison, *U.S. Patent,* 223898 (1880).

5. W. Johnson, L. N. Phillips, and W. Watt, *U.S. Patent,* 3412062 (1966).
6. R. Bacon and W. A. Shalamon, *Appl. Polym. Symp.*, **9**, 285 (1969).
7. A. Shindo, Y. Nakanishi, and I. Soma, *Appl. Polym. Symp.*, **9**, 271 (1969).
8. A. Shindo, *U.S. Patent*, 3529934 (1970).
9. X. Huang, *Materials*, **2**, 2369 (2009).
10. C.-I. Su and C.-L. Wang, *Fiber. Polym.*, **8**, 477 (2007).
11. D. J. Johnson, *J. Phys. D: Appl. Phys.*, **20**, 286 (1987).
12. M. L. Minus and S. Kumar, *J. Minerals, Metals and Materials*, **57**, 52 (2005).
13. D. Zhang and Q. Sun, *J. Appl. Poly. Sci.*, **62**, 367 (1996).
14. A. R. Postema, H. De Groot, and A. J. Pennings, *J. Mat. Sci.*, **25**, 4216 (1990).
15. S. Horikiri, J. Iseki, and M. Minobe, *U.S. Patent*, 4070446 (1978).
16. T.-H. Ko, *U.S. Patent*, 7670970 (2010).
17. W. J. Noss, *U.S. Patent*, 3488151 (1970)
18. U. K. Fatema, C. Tomizawa, M. Harada, and Y. Gotoh, *Carbon*, **49**, 2158 (2011).
19. S.-J. Zhang, H.-Q. Yu, and H.-M. Feng, *Carbon*, **44**, 2059 (2006).
20. Sumitomo Chemical Company Ltd., *British Patent*, 1406378 (1973).
21. H. Ashitaka, Y. Kusuki, S. Yamamoto, Y. Ogata, and A. Nagasaka, *J. Appl. Polym. Sci.*, **29**, 2763 (1984).
22. E. A. Boucher, R. N. Cooper, and D. H. Everett, *Carbon*, **8**, 597 (1970).
23. K. S. Ko, C. W. Park, S.-H. Yoon, and S. M. Oh, *Carbon*, **39**, 1619 (2001).
24. J. A. Newell, D. D. Edie, and E. L. Fuller Jr., *J. Appl. Polym. Sci.*, **60**, 825 (1996).
25. M. C. Blanko Lopez, A. Martinez-Aloso, and J. M. D. Tascon, *Carbon*, **39**, 1177 (2000).
26. M. Shioya, K. Shinotani, and A. Takaku, *J. Mater. Sci.*, **34**, 6015 (1999).
27. K. Kawamura and G. M. Jenkins, *J. Mater. Sci.*, **5**, 262 (1970).
28. D. E. Stuetz, *U.S. Patent*, 3449077 (1969).
29. W. Johnson, R. Moreton, L. N. Phillips, and W. Watt, *French Patent*, 20622005 (1971).
30. Yu. D. Andrichenko and T. V. Druzhinina, *Fiber Chem.*, **31**, 1 (1999).
31. A. V. Tovmash, A. K. Budyka, V. G. Managulashvili, V. A. Rykunov, A. D. Shepelev, and B. I. Ogorodnikov, *Fiber Chem.*, **39**, 450 (2007).
32. J. G. Santangelo, *U.S. Patent*, 3547584 (1970).
33. S. A. El-Garf and S. M. El-Kemry, *Text. Res. J.,* **67**, 13 (1997).
34. S. Dadbin, M. Frounchi, and D. Goudarzi, *Polym. Degrad. Stab.*, **89**, 436 (2005).
35. T. Yang, L. Ye, and Y. Shu, *J. Appl. Polym. Sci.*, **110**, 856 (2008).
36. B. Lanska, L. Matisova-Rychla, and J. Rychla, *Polym. Degrad. Stab.*, **87**, 361 (2005).
37. B. Lanska, L. Matisova-Rychla, and J. Rychla, *Polym. Degrad. Stab.*, **89**, 534 (2005).
38. A. Siegmann and Z. Baraam, *Macromol. Chem., Rapid. Commun.*, **1**, 113 (1980).
39. A. Siegmann and Z. Baraam, *Int. J. Polymeric. Mater.*, **8**, 243 (1980).
40. D. S. Kelkar and N. V. Bhat, *J. Appl. Polym. Sci.*, **43**, 191 (1991).
41. P. Dunn and G. F. Sansom, *J. Appl. Polym. Sci.,* **13**, 1657 (1969).
42. A. Siegmann and Z. Baraam, *Polym. Eng. Sci.*, **21**, 223 (1981).
43. D. S. Kelkar and N. V. Bhat, *J. Phys. D: Appl. Phys.*, **23**, 899 (1990).
44. http://www.oerlikon.com/ecomaXL/index.php?site=OERLIKON_EN_investor_relations_new_otherpublications (LİNK Page # of 873 for Fiber-year-2009-2010 report) (Accessed 28.Nov.2011)
45. A. Lisbao Simal and A. Regina Martin, *J. Appl. Polym. Sci.*, **68**, 441 (1998).
46. X. Liu, Q. Wu, L. A. Berglund, and Z. Qi, *Macromol. Mater. Eng.*, **287**, 515 (2002).
47. M. V. McCabe, *U.S. Patent*, 4661336 (1987).
48. A. M. Hindeleh, D. J. Johnson, and P. E. Montague, "Fibre Diffraction Methods" (A. D. French and K. H. Gardner Eds.), pp.149-181, ACS Symp. No. 141, American Chemical Society, Washington DC, 1983.
49. N. S. Murthy, H. Minor, and C. Bednarczyk, *Macromolecules*, **26**, 1712 (1993).
50. A. M. Hindeleh and D. J. Johnson, *Polymer*, **19**, 27 (1978).
51. N. S. Murthy, S. M. Aharoni, and B. Szollosi, *J. Polym. Sci., Polym. Phys.*, **23**, 2549 (1985).
52. B. L. Deopura in "Polyesters and Polyamides" (B. L. Deopura, R. Alagirusami, M. Joshi, and B. Gupta Eds.), pp.41-60, Woodhead Publishing, Cambridge, UK, 2008.
53. F. Auriemma, V. Petraccone, L. Parravicini, and P. Corradini, *Macromolecules*, **30**, 7554 (1997).
54. L. Penel-Pierron, C. Depecker, R. Seguela, and J.-M. Lefebvre, *J. Polym. Sci. Pol. Phys.*, **39**, 484 (2001).
55. N. Vasanthan, *Text. Res. J.*, **74**, 545 (2004).
56. I. Abu-Isa, *J. Polym. Sci. Pol. Chem.*, **9**, 199 (1971).
57. H. H. Chuah and R. S. Porter, *Polymer*, **27**, 241 (1986).
58. S. Y. Kwak, J. H. Kim, S. Y. Kim, H. G. Jeong, and I. H. Kwon, *J. Polym. Sci. Pol. Phys.,* **38**, 1285 (2000).
59. H. M. Heuvel and R. Huisman, *J. Appl. Polym. Sci.*, **26**, 713 (1981).
60. S. Murase, M. Kashima, K. Kudo, and M. Hirami, *Makromol. Chem. Phys.*, **198**, 561 (1997).
61. Y. Li, L. Cui, F. Guan, Y. Gao, N. E. Hedin, L. Zhu, and H. Fong, *Macromolecules*, **40**, 6283 (2007).
62. N. Vasanthan, *J. Polym. Sci. Pol. Phys.*, **41**, 2870 (2003).
63. L.-C. Chao and E.-P. Chang, *J. Appl. Polym. Sci.*, **26**, 603 (1981).